



ELSEVIER

Contents lists available at ScienceDirect

Journal of Sound and Vibration

journal homepage: www.elsevier.com/locate/jsvi

A robust equal-peak method for uncertain mechanical systems

L. Dell'Elce^{*}, E. Gourc, G. Kerschen

Space Structures and Systems Laboratory, Department of Aerospace and Mechanical Engineering, University of Liege, Liege, Belgium

ARTICLE INFO

Article history:

Received 1 March 2017

Revised 25 September 2017

Accepted 31 October 2017

Available online 14 November 2017

Keywords:

Vibration absorber

Uncertain mechanical system

Equal-peak method

Scenario approach

ABSTRACT

The linear vibration absorber is a widely-used vibration mitigation device. However, when the absorber is tuned according to Den Hartog's equal-peak method, the resulting narrow bandwidth may decrease its effectiveness, especially when the host structure is uncertain or in the presence of environmental variability. In this paper, a new tuning strategy of the linear absorber, based on the concept of robust equal peaks, is introduced for mitigating a specific resonance of an uncertain mechanical system. Both analytical and numerical investigations are carried out to demonstrate the robustness of the proposed absorber. For 20% uncertainty in the stiffness of the host system, the performance improvement brought by the robust equal-peak method amounts to more than 30% with respect to Den Hartog's tuning rule.

© 2017 Elsevier Ltd. All rights reserved.

1. Introduction

The use of linear resonators for the mitigation of resonant vibrations was first proposed by Watts [1] and Frahm [2,3] to reduce the rolling motion of ships. The problem was later formalized in more rigorous terms by Ormondroyd and Den Hartog [4], Den Hartog [5] and Brock [6], who developed tuning rules that formed the basis of *Den Hartog's equal-peak method*. The vibration absorber considered in Refs. [4–6] consists of a mass-spring-dashpot system attached to the primary system to be controlled. Through the proper tuning of the absorber's spring and dashpot, it is possible to approximately obtain h_∞ optimization of the frequency response in the vicinity of the target resonance frequency.

Thanks to its simplicity, effectiveness, low cost and small requirements for maintenance [7], the linear vibration absorber (often referred to as tuned mass damper, tuned vibration absorber or dynamic vibration absorber) was implemented in various real-life structures. Its main applications include structures subject to human-induced vibrations, such as spectator stands and pedestrian bridges (the most famous example is the Millenium bridge in London [8]), steel structures excited by machines such as centrifuges and fans, aircraft engines [9], helicopter rotors [10], tall and slender structures subject to wind-induced vibrations, but also power lines [11] and long-span suspended bridges [12,13]. For a list of installations of vibration absorbers in civil structures, the interested reader can refer to [14,15].

An overview of existing designs for passive vibration absorbers is given in Ref. [7]. They include classical absorbers with translational mass movements, pendulum absorbers, centrifugal pendulum absorbers [16], ball absorbers, sloshing liquid absorbers [17] and particle vibration absorbers [18], although the sloshing liquid and particle vibration absorbers have qualitatively different features than the more typical vibration absorbers with a concentrated mass. Many different configurations and variations of the original vibration absorber were studied in the last decades, e.g., a damped host system [19], different combinations of

^{*} Corresponding author. Space Structures and Systems Laboratory, Department of Aerospace and Mechanical Engineering, University of Liege, Alle de la Decouverte 9 (B52/3), B-4000, Liège, Belgium.

E-mail addresses: lamberto.dellelce@ulg.ac.be (L. Dell'Elce), etienne.gourc@gmail.com (E. Gourc), g.kerschen@ulg.ac.be (G. Kerschen).

response and excitation [20] and the use of multi-vibration absorbers to control several resonances [21].

A fundamental drawback of the linear tuned vibration absorber (LTVA) is that it requires a fine tuning between its natural frequency and the targeted resonance frequency. The LTVA may therefore lose efficiency in the presence of uncertainty [22–24] or nonlinearity [25]. In this context, the main contribution of this paper is to revisit the tuning strategy of a LTVA attached to a primary system with uncertain stiffness and damping. As in previous studies [22,24,26,27], a min-max formulation is adopted; it is solved using the scenario approach [28], a recently-introduced robust optimization method. The careful analysis of the results obtained through the scenario approach brings new insight into the problem which gives rise to the concept of *robust equal peaks* introduced in this paper.

The paper is organized as follows. Section 2 briefly reviews Den Hartog's equal-peak method and the detuning of the LTVA when attached to an uncertain system. In Section 3, the absorber tuning strategy is formulated as a worst-case design problem; the scenario approach is also presented. Section 4 introduces the concept of robust equal peaks and provides numerical and analytical solutions for tuning the robust LTVA. Section 5 discusses the validity and limitations of the proposed tuning strategy. The conclusions of the present study are summarized in Section 6.

2. The linear tuned vibration absorber: equal-peak method

The steady-state response of an undamped mass-spring system subjected to harmonic excitation at a constant frequency can be suppressed using an undamped LTVA, as proposed by Frahm in 1909 [2]. However, LTVA performance deteriorates significantly when the excitation frequency varies. To improve robustness, damping was introduced in the absorber by Ormondroyd and Den Hartog [4]. Denoting by k_1 and c_1 the stiffness and damping of the primary system and by k_2 and c_2 their analogous of the absorber, the equations of motion of the coupled system are

$$\begin{aligned} m_1 \ddot{x}_1 + k_1 x_1 + c_2 (\dot{x}_1 - \dot{x}_2) + k_2 (x_1 - x_2) &= f(t) \\ m_2 \ddot{x}_2 + c_2 (\dot{x}_2 - \dot{x}_1) + k_2 (x_2 - x_1) &= 0 \end{aligned} \quad (1)$$

and their counterpart in the frequency domain is

$$\begin{bmatrix} k_1 + k_2 + i\omega(c_1 + c_2) - \omega^2 m_1 & -(k_2 + i\omega c_2) \\ -(k_2 + i\omega c_2) & k_2 + i\omega c_2 - \omega^2 m_2 \end{bmatrix} \begin{Bmatrix} X_1 \\ X_2 \end{Bmatrix} = \begin{Bmatrix} F(\omega) \\ 0 \end{Bmatrix} \quad (2)$$

where $X_1(\omega)$ and $X_2(\omega)$ are the displacements of the harmonically-forced primary system and of the damped LTVA, respectively. Den Hartog realized that the receptance function of the primary mass, i.e., $h_1 = \frac{X_1(\omega)}{F(\omega)}$, passes through two invariant points independent of absorber damping. He proposed to adjust the absorber stiffness to have two fixed points of equal heights in the receptance curve and to select the absorber damping so that the curve presents a horizontal tangent through one of the fixed points. This laid down the foundations of the so-called *equal-peak method*, widely used in practical applications [29]. As illustrated in Fig. 1, the equal-peak method minimizes the maximum amplitude response of the primary system, corresponding to H_∞ optimization.

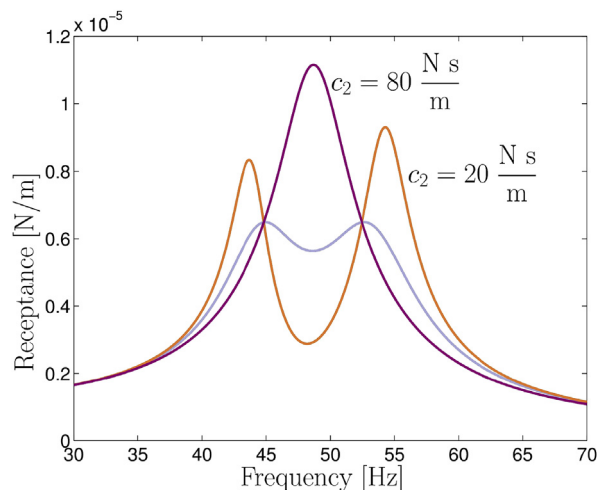


Fig. 1. Illustration of Den Hartog's equal-peak method, $\omega_1 = 50$ Hz, $m_1 = 10$ kg, $\eta = 0.05$. Equal peaks are obtained for $k_2 = 4.48e4$ N/m and $c_2 = 39.98$ N s/m.

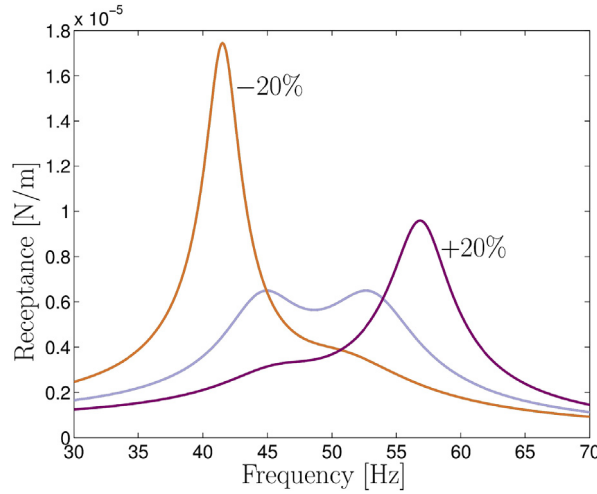


Fig. 2. LTVA detuning for 20% variation in the primary system's stiffness k_1 .

Den Hartog [5] and Brock [6] derived approximate analytical formulas for the absorber stiffness and damping, respectively:

$$\frac{\omega_2}{\omega_1} = \sqrt{\frac{k_2 m_1}{k_1 m_2}} = \frac{\eta}{1 + \eta}$$

$$\xi_2 = \frac{c_2}{2\sqrt{k_2 m_2}} = \sqrt{\frac{3}{8(1 + \eta)}} \tag{3}$$

where ω_1 and ω_2 are the natural frequencies of the primary system and of the absorber, respectively, $\eta = m_2/m_1$ is the mass ratio and ξ_2 is the damping ratio of the absorber.

Interestingly, it is only recently that an exact closed-form solution to this classical problem could be found [30]:

$$\frac{\omega_2}{\omega_1} = \frac{2}{1 + \eta} \sqrt{\frac{2 \left[16 + 23\eta + 9\eta^2 + 2(2 + \eta)\sqrt{4 + 3\eta} \right]}{3(64 + 80\eta + 27\eta^2)}}$$

$$\xi_2 = \frac{c_2}{2\sqrt{k_2 m_2}} = \frac{1}{4} \sqrt{\frac{8 + 9\eta - 4\sqrt{4 + 3\eta}}{1 + \eta}}$$
(4)

When the primary system is uncertain, the performance of the equal-peak method can quickly deteriorate. For instance, for 20% uncertainty in the primary system's stiffness k_1 , Fig. 2 shows that the maximum peak amplitude can increase by almost 200%. The objective of this paper is therefore to revisit the equal-peak method in the presence of uncertainty.

3. Worst-case design of the linear tuned vibration absorber

3.1. Problem statement

In this section, the tuning of the LTVA for a primary system with uncertain stiffness and damping is formulated as a *worst-case optimization problem*. Hence, the LTVA that minimizes the maximum response amplitude of the primary system among all possible outcomes of the uncertain set is sought:

$$[c_2^*, k_2^*] = \arg \left[\min_{c_2, k_2 \in \mathbb{R}^+} \left(\max_{[c_1, k_1] \in \Delta} |h_1(\omega)|_{m_1, c_1, k_1, m_2, c_2, k_2} \Big|_{\infty} \right) \right], \tag{5}$$

where $|h_1(\omega)|_{\infty}$ denotes the *H-infinity* norm of the receptance (ω) of the primary system, and Δ represents the sample space.

3.2. The scenario approach

Problem (5) is solved in Section 4.1 by means of the scenario approach, a general-purpose numerical method for robust

optimization [28,31]. Here, we briefly recall the mathematical foundations of this technique.

Consider the robust optimization problem

$$\mathbf{y}^* = \arg \left[\min_{\mathbf{y}} (\mathbf{c}^T \mathbf{y}) \right] \quad \text{s.t. :} \quad \mathbf{g}(\mathbf{y}, \delta) \leq \mathbf{0} \quad \forall \delta \in \Delta. \tag{6}$$

where \mathbf{y} is the d -dimensional vector of design variables, $\delta \in \Delta$ is a generic random quantity with probability distribution p_Δ , \mathbf{c} is a constant vector, and \mathbf{g} is a set of convex constraints with respect to \mathbf{y} . The optimal solution of Problem (6), denoted by \mathbf{y}^* , is robust all over the uncertain domain Δ . Hence, \mathbf{y}^* is feasible for any sample $\delta \in \Delta$, i.e., $\mathbf{g}(\mathbf{y}^*, \delta) \leq \mathbf{0}$.

When the event space of Δ is a dense set – as it is most often the case – solving Problem (6) is challenging because an infinite number of constraints have to be enforced. The scenario approach solves a relaxed version of Problem (6), where the obtained solution is only feasible in a subset of Δ such that the probability that a realization of the uncertain quantities belongs to this subset is larger than a desired threshold $1 - \epsilon$. Here $\epsilon \in (0, 1]$ is referred to as *risk parameter*. The extreme cases $\epsilon = 1$ and $\epsilon = 0^+$ are associated to the solution of a deterministic problem (uncertainty is neglected) and of the original robust optimization Problem (6), respectively.

The main theorem of the scenario approach [32] states that, given the confidence level $\beta \in [0, 1)$, the risk parameter ϵ , and n independent instances $(\delta_1, \dots, \delta_n)$ of Δ extracted according to p_Δ and such that n satisfies

$$\sum_{i=0}^{d-1} \frac{n!}{i!(n-i)!} \epsilon^i (1-\epsilon)^{n-i} \leq \beta, \tag{7}$$

the solution of the *finite*-dimensional problem

$$\mathbf{y}^{(s)} = \arg \left[\min_{\mathbf{y}} (\mathbf{c}^T \mathbf{y}) \right] \quad \text{s.t. :} \quad \mathbf{g}(\mathbf{y}, \delta) \leq \mathbf{0} \quad \forall \delta \in (\delta_1, \dots, \delta_n) \tag{8}$$

satisfies, with probability not smaller than $1 - \beta$, all unseen constraints in Δ except for a fraction ϵ of Δ , i.e.,

$$\begin{aligned} \exists \Delta_s \subset \Delta \quad \text{s.t.} \quad & \Pr(\mathbf{g}(\mathbf{y}^{(s)}, \delta) \leq \mathbf{0}, \quad \forall \delta \in \Delta_s) \geq 1 - \beta \\ & \Pr(\Delta_s) \equiv \int_{\Delta_s} p_\Delta(\delta) \, d\delta \geq 1 - \epsilon \end{aligned} \tag{9}$$

The theorem is illustrated schematically in Fig. 3: by randomly extracting n samples from the uncertain set it is possible to guarantee with a desired confidence, $1 - \beta$, that the solution obtained by enforcing the constraints *only* for these samples (i.e., a finite number of constraints) is feasible on a dense subset Δ_s which is at least a ‘portion’ $1 - \epsilon$ of Δ . We further emphasize that both ϵ and β are chosen *a priori*.

Thanks to the replacement of Problem (6) with Problem (8), the solution becomes easily tractable using classical optimization algorithms. However, based on the n instances or *scenarios* considered during the optimization, the solution is only guaranteed with probability $1 - \beta$ in the subset Δ_s , the size of which is governed by the user-defined parameter ϵ . A conservative bound of Equation (7) which gives an explicit expression of n as a function of ϵ and β is [33]

$$n \geq \frac{2}{\epsilon} (d - \ln \beta) \tag{10}$$

Enforcing β to zero requires an infinite number of scenarios. However, because β appears as the argument of a logarithm, it can be taken as small as desired, e.g., $\beta = 1e - 10$, without substantially increasing the required number of scenarios. The probability that the solution is verified in the subset Δ_s is thus virtually equal to 1.

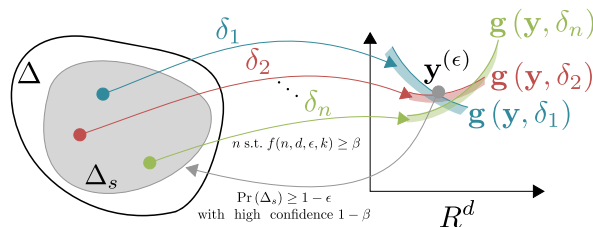


Fig. 3. Schematic representation of the scenario approach.

Depending on the application at hand, the theorem may yield very conservative solutions, i.e., the probability of the subset where the constraints are violated by the computed solution $\mathbf{y}^{(s)}$ can be much smaller than ϵ . The sampling-and-discarding theorem overcomes this issue [34]: for a solution with risk ϵ , the greatest number of samples j that can be removed from a set of n samples obeys the relation

$$\frac{j+d-1!}{j!(d-1)!} \sum_{i=0}^{j+d-1} \frac{n!}{i!(n-i)!} \epsilon^i (1-\epsilon)^{n-i} \leq \beta. \tag{11}$$

Interestingly, the removed samples can be selected according to any arbitrary criterion. So, in practice, for a given risk, if n is chosen as large as possible according to the available computational resources, the j removed samples should violate the solution $\mathbf{y}^{(s)}$, so that very similar *a priori* and *a posteriori* violation sets are obtained.

4. The concept of robust equal peaks

The design of a robust LTVA is first tackled in this section by means of the scenario approach with the sampling-and-discarding theorem. The parameter β is set to $1e - 10$ in all simulations. An analytical solution to the obtained numerical solution is then sought.

Table 1 lists the parameters of the primary system and the considered mass ratio. The damping and stiffness of the primary system are statistically independent random variables with uniform marginal distributions. Specifically, a 20% uncertainty is considered for the stiffness, and the damping ratio is allowed to vary between 0 and 1%.

Table 2 is introduced to facilitate the connection between Section 3.2 and the notation used in the remainder of the paper.

4.1. Numerical solution using the scenario approach

The cost function of Problem (6) is linear with respect to the design variables. For this reason, we introduce an auxiliary variable, h , to recast Problem (5) into the form of Problem (6):

$$\begin{aligned} [c_2^*, k_2^*, h^*] &= \arg \left(\min_{c_2, k_2, h \in \mathbb{R}^+} h \right) \quad \text{s.t. :} \\ |h_1(\omega | m_1, c_1, k_1, m_2, c_2, k_2)|_{\infty} &\leq h \quad \forall [c_1, k_1] \in \Delta. \end{aligned} \tag{12}$$

The optimum value of h , namely h^* , is identified by solving the optimization problem (analogously to c_2^* and k_2^*), and it represents the worst-case magnitude of the *H-infinity* norm of the receptance function h_1 .

Fig. 4(a) presents the evolution of the optimal solution h^* as a function of the risk. It appears that h^* does not exceed $1.2e - 5$ m/N, a 30% improvement with respect to the classical LTVA (see Fig. 2). The optimal variable h^* in the chance-constrained problem is associated to the worst realization of h_1 among all possible values of the uncertain parameters in Δ_ϵ , which is a subset of Δ . Hence, h^* monotonically decreases with the risk ϵ because the size of the set Δ_ϵ also decreases. However, if the

Table 1
Parameters considered for the design of the robust LTVA. $\mathcal{U}(a, b)$ denotes the uniform distribution with support $[a, b]$; the tilde means "distributed according to".

Parameter	Value
m_1	10 kg
m_2	0.5 kg
$\omega_1 / (2\pi)$	50 Hz
ξ_1	0.01
c_1	$\sim \mathcal{U}(0, 2 m_1 \omega_1 \xi_1)$
k_1	$\sim \mathcal{U}(0.8 m_1 \omega_1^2, 1.2 m_1 \omega_1^2)$
$\text{corr}(C_1, K_1)$	0

Table 2
Analogy between the notations used in Section 3.2 and 4.1.

Section 3.2	Section 4.1
\mathbf{y}	$[c_2, k_2, h]$
\mathbf{c}	$[0, 0, 1]$
d	3
δ	$[c_1, k_1]$
Δ	$[0, 2 m_1 \omega_1 \xi_1] \times [0.8 m_1 \omega_1^2, 1.2 m_1 \omega_1^2]$
p_Δ	Uniform distribution

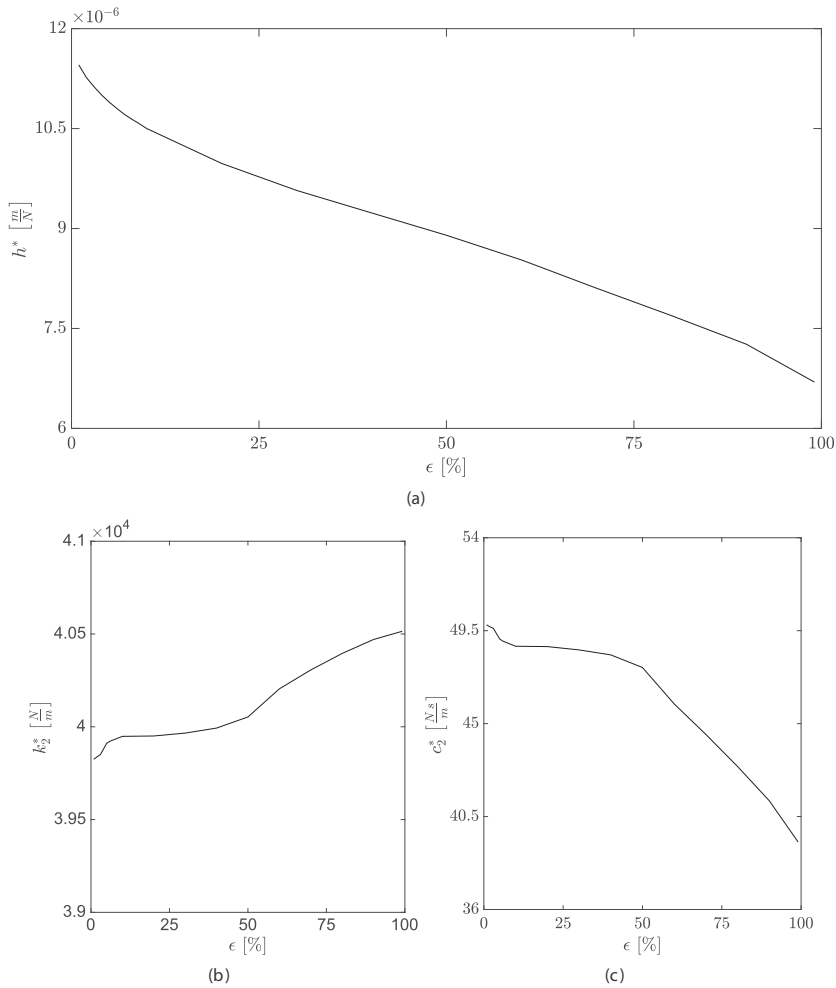


Fig. 4. Optimal absorber as a function of the risk ϵ . The performance index is illustrated in (a). Figures (b) and (c) depict the absorber's stiffness and damping, respectively.

actual value of the uncertain parameters lie in the violation set, the H -infinity norm of h_1 is greater than h^* . To better clarify this point, consider the extreme case $\epsilon = 1$. When the risk is maximum, the design of the absorber ignores the uncertainty. Hence, the absorber is designed by using the classical equal peaks concept with the nominal values of the parameters of the primary system. In this case, h^* is the H -infinity norm of the nominal response function (tuned curve of Fig. 2). Fig. 4(b–c) plot the corresponding damping and stiffness coefficients of the robust LTVA. For small risks, k_2^* and c_2^* take values around $k_2 = 4e4$ N/m and $c_2 = 50$ N s/m, respectively, which are to be compared to those obtained using Den Hartog's equal peak method, i.e., $k_2 = 4.48e4$ N/m and $c_2 = 39.98$ N s/m.

Further insight into the obtained solution can be gained by analyzing the violation set. To this end, we first consider the 10% risk solution for which h^* was found to be $8.39e-6$ m/N. Fig. 5, which illustrates the value $|h_1(\omega)|_\infty$ in the whole uncertain set, clearly shows that values greater than h^* are obtained in the top- and bottom-left corners. Constraint violation therefore occurs at the extremity of the stiffness' uncertainty interval and for the smallest damping values. This finding is confirmed by looking at the evolution of the violation set as a function of the risk. Fig. 6 reveals that the violation set is more and more squeezed toward the top- and bottom-left corners as risk approaches 0.

The receptance curves of the samples used to compute the 10% risk-guaranteed solution, depicted in Fig. 7, also convey important information. It turns out that the two worst samples, located close to the two extremities of the stiffness' uncertainty interval, present resonance peaks with identical amplitude.

Summarizing, these results suggest the concept of *robust equal peaks* which considers only two samples $k_1^{(\min)}, c_1^{(\min)}$ and $k_1^{(\max)}, c_1^{(\min)}$ in the sample space Δ :

The solution of the original worst-case Problem (12) is such that the amplitude of the leftmost resonance peak of sample $k_1^{(\min)}, c_1^{(\min)}$ should be equal to the amplitude of the rightmost resonance peak of sample $k_1^{(\max)}, c_1^{(\min)}$.

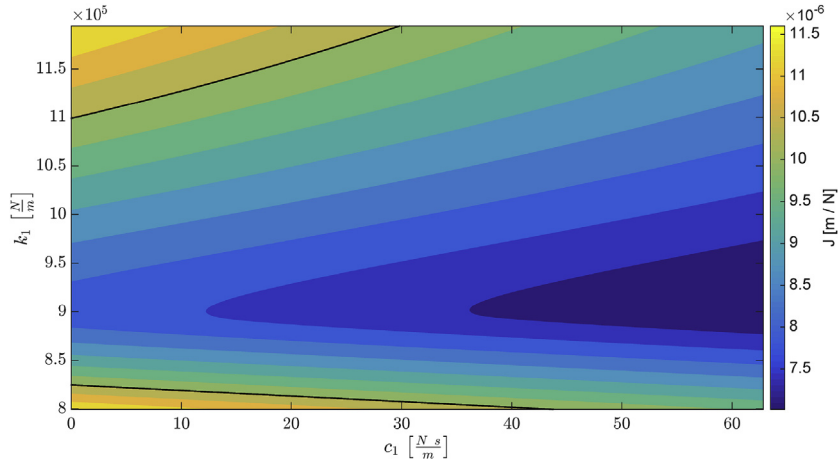


Fig. 5. $|h_1(\omega)|_\infty$ in the uncertain set for the 10% risk-guaranteed absorber. The black line delimits the boundary of the violation set.

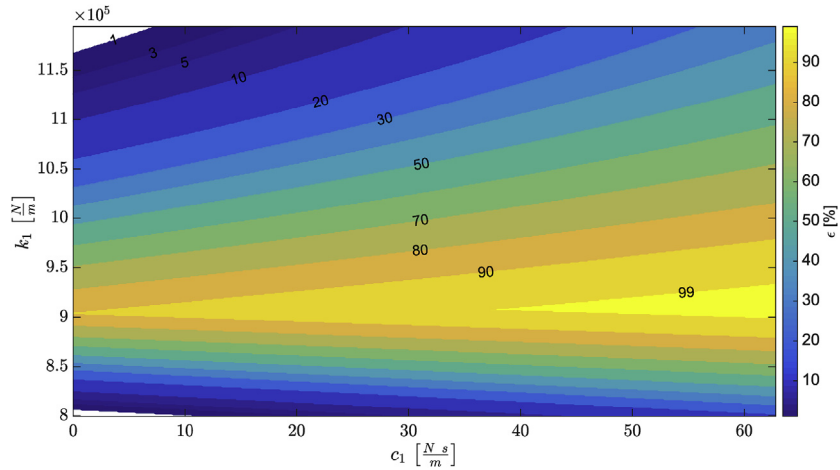


Fig. 6. Violation set as a function of the risk ϵ .

Mathematically,

$$\begin{aligned}
 [c_2^*, k_2^*, h^*] &= \arg \left(\min_{c_2, k_2, h \in \mathbb{R}^+} h \right) \quad \text{s.t. :} \\
 \left| h_1 \left(\omega | m_1, c_1^{(\min)}, k_1^{(\min)}, m_2, c_2, k_2 \right) \right|_\infty &= h, \\
 \left| h_1 \left(\omega | m_1, c_1^{(\min)}, k_1^{(\max)}, m_2, c_2, k_2 \right) \right|_\infty &= h.
 \end{aligned} \tag{13}$$

Although nonlinear, Problem (13) has just two equality constraints and can be efficiently solved using classical optimizers. The solution found is $k_2 = 3.97e4$ N/m and $c_2 = 50.39$ N s/m.

We finally note that the concept of robust equal peaks holds for a given bounded event space, Δ , regardless of the specific probability distribution, p_Δ . This conjecture is further discussed in Section 5.

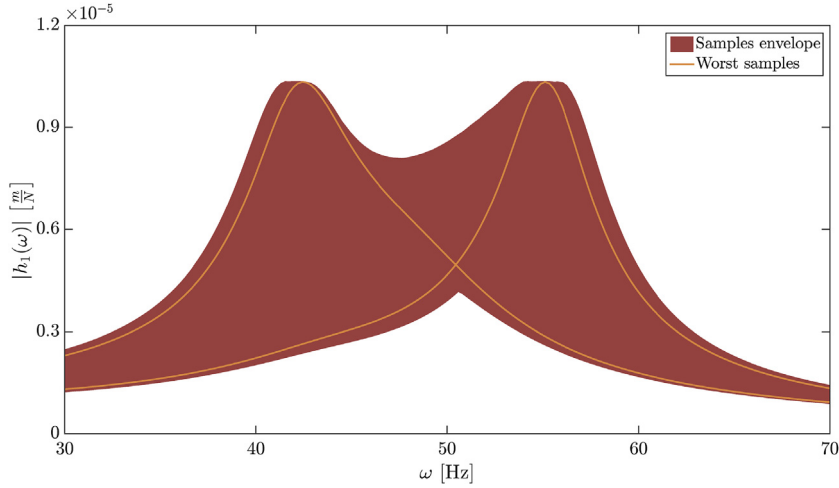


Fig. 7. Receptance curves of the samples used at $\epsilon = 0.1$. The red-shaded region defines the envelope of the samples. The orange lines represent the worst samples. (For interpretation of the references to colour in this figure legend, the reader is referred to the web version of this article.)

4.2. An analytical solution

The previous section has shown that an undamped primary system corresponds to the worst-case scenario, meaning that damping uncertainty can be safely neglected. The stiffness is defined on the bounded support $[k^{(\min)}, k^{(\max)}]$.

We adopt the notations

$$\bar{\omega}_1 = \sqrt{\frac{k_1^{(\max)} + k_1^{(\min)}}{2m_1}}, \quad \eta = \frac{m_2}{m_1}, \quad \nu = \frac{k_1^{(\max)} - k_1^{(\min)}}{k_1^{(\max)} + k_1^{(\min)}} \quad (14)$$

for the nominal resonance frequency, the mass ratio, and the relative range of the stiffness, respectively, and

$$\lambda = \frac{c_2}{m_2\bar{\omega}_1}, \quad \rho = \frac{k_2}{m_2\bar{\omega}_1^2} \quad (15)$$

are the dimensionless parameters of the absorber. Defining $\theta = \omega/\bar{\omega}_1$ the dimensionless pulsation, the equations of motion (2) become

$$\begin{bmatrix} (1 + \delta) + \eta\rho + i\theta\eta\lambda - \theta^2 & -\eta(\rho + i\theta\lambda) \\ -(\rho + i\theta\lambda) & \rho + i\theta\lambda - \theta^2 \end{bmatrix} \begin{Bmatrix} X_1 \\ X_2 \end{Bmatrix} = \frac{1}{m_1\bar{\omega}_1^2} \begin{Bmatrix} F(\theta) \\ 0 \end{Bmatrix} \quad (16)$$

where $\delta \in [-\nu, \nu]$ is the random variable modeling the stiffness uncertainty. The objective of the tuning strategy developed herein is to find analytical values of ρ and λ for a given mass ratio η so as to solve the robust equal-peak Problem (13).

The absolute value of the dimensionless receptance function is

$$\left| \tilde{h}_1(\theta|\lambda, \rho, \eta, \delta) \right| = \left| \frac{h_1}{m_1\bar{\omega}_1^2} \right| = \sqrt{\frac{\theta^2\lambda^2 + \theta^2 - \rho}{a(\theta|\eta, \delta)\lambda^2 + b(\theta|\rho, \eta, \delta)}}, \quad (17)$$

where

$$a(\theta|\eta, \delta) = \theta^2[\theta^2(1 + \eta) - 1 - \delta]^2, \quad (18)$$

$$b(\theta|\rho, \eta, \delta) = \{\theta^4 - \theta^2[\rho(1 + \eta) + 1 + \delta] + \rho(1 + \delta)\}^2.$$

According to the theory of the classical equal-peak method, for given ρ , η , and δ , the receptance curve exhibits two fixed points p and q for varying λ , as illustrated in Fig. 8. Their abscissas, θ_p and θ_q , are such that Equation (17) is independent of λ . This occurs when

$$\theta_{p,q}^2 b(\theta_{p,q}|\rho, \eta, \delta) = (\theta_{p,q}^2 - \rho) a(\theta_{p,q}|\eta, \delta). \quad (19)$$

Solving Equation (19) for $\theta_{p,q}$ yields

$$\theta_{p,q}^2 = \frac{\rho(1 + \eta) + 1 + \delta \mp \sqrt{\rho^2(1 + \eta)^2 - 2\rho(1 + \delta) + (1 + \delta)^2}}{\eta + 2}. \quad (20)$$

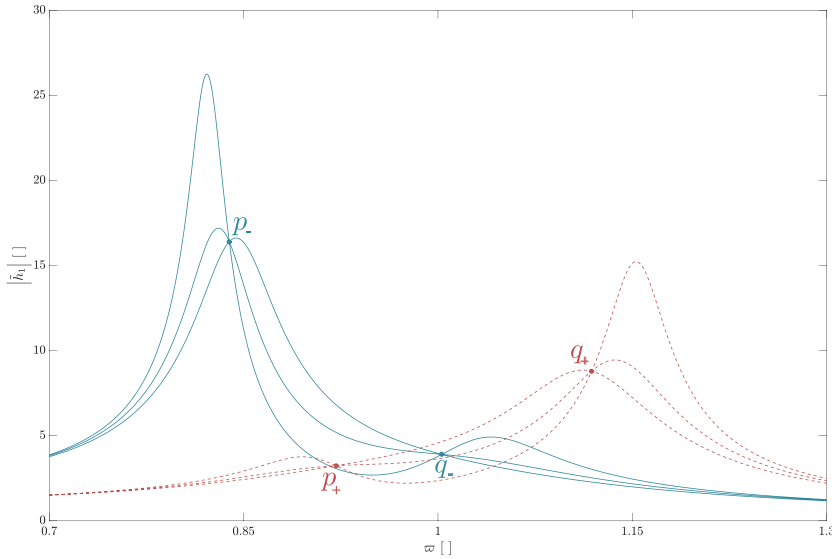


Fig. 8. Receptance curves for the parameters listed in Table 1. Blue and orange curves correspond to $\delta = \mp 0.2$, respectively. Dash-dotted, solid and dashed lines correspond to different absorber damping values. (For interpretation of the references to colour in this figure legend, the reader is referred to the web version of this article.)

The ordinates of the fixed points can be evaluated by means of Equation (17) for any arbitrary damping value λ . Manipulations are simplified using $\lambda \rightarrow \infty$, so that

$$\left| \tilde{h}_1(\theta_{p,q} | \infty, \rho, \eta, \delta) \right|^2 = \frac{1}{\theta_{p,q}^2 (1 + \eta) - 1 - \delta}. \tag{21}$$

Following the robust equal-peak tuning strategy, only the two samples corresponding to $\delta = \pm \nu$ have to be considered. Their receptance curve possesses two fixed points denoted p_- and q_- for $\delta = -\nu$, and p_+ and q_+ for $\delta = \nu$. As illustrated in Fig. 8, the optimal stiffness of the robust LTVA ρ^* is obtained by imposing equal ordinates to the fixed points p_- and q_+ .

$$\left| \tilde{h}_1(\theta_{p_-} | \infty, \rho^*, \eta, -\nu) \right| = \left| \tilde{h}_1(\theta_{q_+} | \infty, \rho^*, \eta, \nu) \right|, \tag{22}$$

Substituting Equations (20) and (21) into Equation (22) and solving for ρ^* results in

$$\rho^* = \frac{1 - \nu \sqrt{\nu^2(1 + \eta)^2 + \eta(\eta + 2)}}{(\nu^2 + 1)(1 + \eta)^2}. \tag{23}$$

As in the classical equal-peak method, damping is determined by imposing horizontal tangents at p_- and q_+ . Differentiating Equation (17) with respect to θ yields

$$\frac{d \left| \tilde{h}_1 \right|^2}{d\theta} = a_2 \lambda^4 + a_1 \lambda^2 + a_0, \tag{24}$$

where

$$\begin{aligned} a_2 &= -2\theta^3 (1 + \eta) \sqrt{a(\theta|\eta, \delta)}, \\ a_1 &= -4\theta\rho^2 (1 + \eta) \sqrt{a(\theta|\eta, \delta)} - \theta^6 [\theta^2 (\eta^2 + 2\eta + 4) - 4(1 + \delta)] + 2\theta^4 \rho [2\theta^2 (\eta^2 + 3\eta + 2) - (3\eta + 4)(1 + \delta)], \\ a_0 &= -2(\theta^2 - \rho) [\theta^4 + \rho^2 (1 + \eta) - 2\theta^2 \rho] \sqrt{b(\theta|\rho, \eta, \delta)} \end{aligned} \tag{25}$$

Table 3
Absorber parameters for the classical and robust equal-peak methods, $\nu = 0.2$.

Parameter	Classical	Robust – numerical	Robust – analytical
k_2	4.48e4 N/m	3.97e4 N/m	3.97e4 N/m
c_2	39.98 N s/m	50.39 N s/m	52.37 N s/m

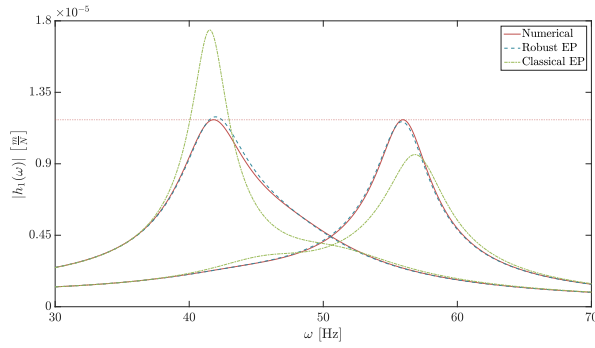


Fig. 9. Comparison between numerical and analytical implementation of the robust equal peaks.

Evaluating Equations (24) and (25) for p_- and q_+ and solving

$$\left. \frac{d|\tilde{h}_1|^2}{d\theta} \right|_{\theta=\theta_{p_-,q_+}} = 0 \tag{26}$$

for λ^2 yields λ_{p_-} and λ_{q_+} . Closed-form expression of Equation (26) is

$$a_2^{(p_-,q_+)} \lambda_{p_-,q_+}^4 + a_2^{(p_-,q_+)} \lambda_{p_-,q_+}^2 + a_0^{(p_-,q_+)} = 0, \tag{27}$$

with

$$\begin{aligned} a_2^{(p_-,q_+)} &= -2\theta_{p_-,q_+}^4 (1 + \eta) \left[\theta_{p_-,q_+}^2 (1 + \eta) - 1 \pm \nu \right], \\ a_1^{(p_-,q_+)} &= -4\theta_{p_-,q_+}^2 \rho^{*2} (1 + \eta) \left[\theta_{p_-,q_+}^2 (1 + \eta) - 1 \pm \nu \right] - \theta_{p_-,q_+}^6 \left[\theta_{p_-,q_+}^2 (\eta^2 + 2\eta + 4) - 4(1 \mp \nu) \right] \\ &\quad + 2\theta_{p_-,q_+}^4 \rho^* \left[2\theta_{p_-,q_+}^2 (\eta^2 + 3\eta + 2) - (3\eta + 4)(1 \mp \nu) \right], \\ a_0^{(p_-,q_+)} &= -2 \left(\theta_{p_-,q_+}^2 - \rho^* \right) \left[\theta_{p_-,q_+}^4 + \rho^{*2} (1 + \eta) - 2\theta_{p_-,q_+}^2 \rho^* \right] \left\{ \theta_{p_-,q_+}^4 - \theta_{p_-,q_+}^2 [\rho^* (1 + \eta) \mp \nu + 1] + \rho^* (1 \mp \nu) \right\}, \\ \theta_{p_-,q_+}^2 &= \frac{\rho^* (1 + \eta) + 1 \mp \nu \mp \sqrt{\rho^{*2} (1 + \eta)^2 - 2\rho^* (1 \mp \nu) + (1 \mp \nu)^2}}{\eta + 2}. \end{aligned} \tag{28}$$

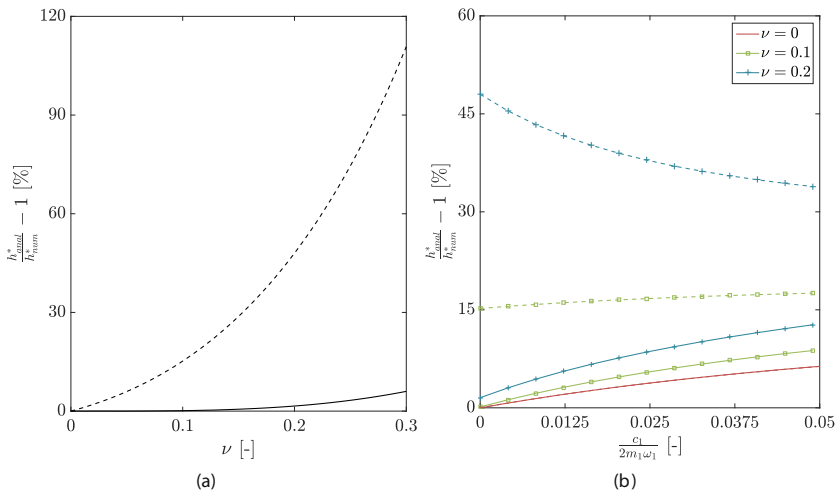


Fig. 10. Performance of the analytical rule as a function of stiffness detuning (a) and of primary's damping (b). Dashed lines are computed by using the classical Den Hartog's rule (Equation (3)). Solid lines use the analytical robust equal peaks tuning rule (Equation (29)).

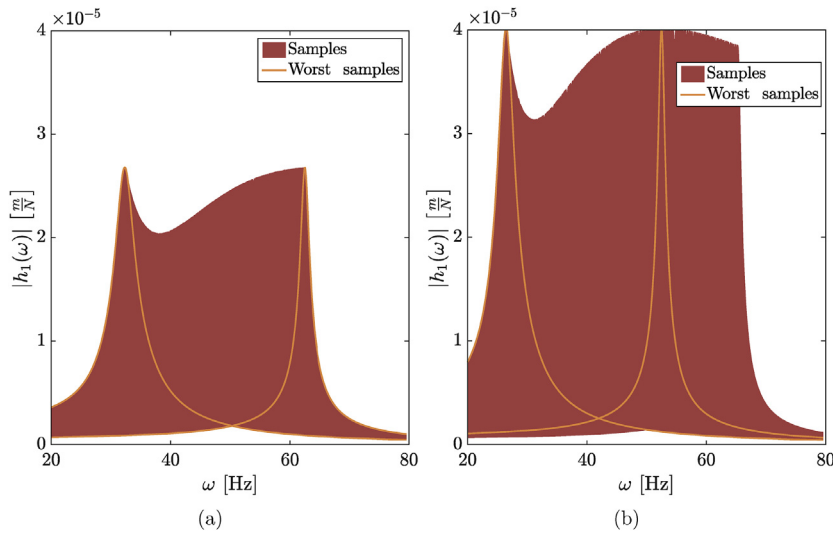


Fig. 11. Samples used by the scenario approach for very large uncertainty in the primary system' stiffness, namely 55% (a) and 70% (b). The risk parameter is set to $\epsilon = 0.1$.

Equation (27) has always a positive and a negative solution for physically meaningful systems. The positive value is systematically chosen. The optimum value of the damping parameter is taken as their average, $\frac{\lambda_{p-} + \lambda_{q+}}{2}$, so that the dimensional optimal parameters of the absorber are

$$k_2^* = m_2 \bar{\omega}_1^2 \rho^*, \quad c_2^* = m_2 \bar{\omega}_1 \frac{\lambda_{p-} + \lambda_{q+}}{2}. \tag{29}$$

For the parameters listed in Table 1, Table 3 compares the absorber coefficients calculated numerically through Equation (13) and analytically through the classical (3) and robust (29) equal-peak methods. The corresponding receptance curves in Fig. 9 confirm the important detuning of the classical equal-peak method and also shows that the proposed analytical solution presents only a very slight deviation from the numerical solution. A more quantitative assessment for various uncertainty levels is provided in Fig. 10. For large uncertainty ($\nu = 0.3$), the error of the analytical rule is barely 6% whereas the error given by classical equal-peak method amounts to 110%.

The error when the lower bound of the damping is not zero is depicted in Fig. 10(b). Unsurprisingly, the predictive capability of the analytical formulas obtained for an undamped primary system deteriorates. However, the error remains below 10% even for a lower bound of the damping ratio of 2%.

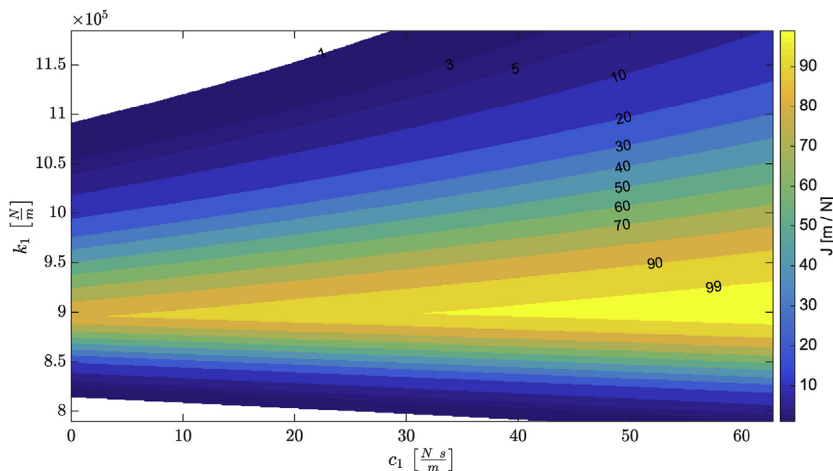


Fig. 12. Violation set in function of the risk ϵ when the damping and stiffness of the primary system are noncorrelated truncated Gaussian random variables.

5. Further considerations

This section further investigates the validity of the concept of robust equal peaks. Specifically, we first analyze whether the concept still holds for an arbitrarily large uncertain set. If the uncertainty in the primary system' stiffness is increased up to 55%, Fig. 11(a) shows that equal peaks still hold between the two samples located at the extremes of the stiffness' uncertainty interval. However, it can be observed that the envelope of the samples reaches a plateau at the right extremity of the interval. Increasing the uncertainty further, i.e., to 70% as in Fig. 11(b), equal peaks occur between two samples which are not at the extremes of the uncertainty interval. For this fairly unrealistic uncertainty, the numerical and analytical solutions obtained through Equations (13) and (29), respectively, can no longer be exploited, but the risk-guaranteed absorber can still be designed by means of the scenario approach.

The influence of the joint probability distribution p_{Δ} is now examined. Fig. 12 depicts the violation set in the case of truncated Gaussian distributions. Even if the violation set seems to shrink at a slower pace, this figure presents qualitatively the same features as for the uniform distribution in Fig. 6. For a bounded but non-rectangular distribution, one should remark that imposing equal peaks at the extremes of the uncertainty interval yields a slightly conservative solution in terms of receptance h^* , because the outer rectangle encompassing the original event space is considered. Finally, for an unbounded Gaussian distribution, robust equal peaks cannot be strictly imposed. Risk-guaranteed solutions can still be computed using the scenario approach, but a good approximation to the worst-case solution will require a very small risk, and, hence, a large computational burden. To alleviate it, the convex hull of the samples can be considered or even just the extreme stiffness and lowest damping of the samples themselves.

6. Conclusion

The objective of this paper was to develop a new tuning strategy for linear vibration absorbers in the case of uncertain resonances. Specifically, for H_{∞} minimization of the receptance curve, we have shown that the amplitude of the leftmost resonance peak of the sample associated with minimum stiffness and damping should be equal to the amplitude of the rightmost resonance peak of the sample associated with the maximum stiffness and minimum damping. This problem can be solved either numerically through a simple minimization problem with equality constraints, i.e., Equation (13), or analytically using Equation (29). This tuning strategy, termed the robust equal-peak method, provides a generalization of Den Hartog's equal-peak method in the presence of uncertainty in the primary system.

Acknowledgments

This work was supported by the Belgian National Fund for Scientific Research (FNRS), the Marie Curie BEIPD-COFUND programme at the University of Liège, Belgium, and by the French National Center for Space Studies (CNES), R&T RS14/TG-002-096. The Authors thank Ms. G. Aridon and Prof. G. Michon for the useful discussions in the framework of this project.

References

- [1] P. Watts, On a method of reducing the rolling of ships at sea, *Trans. Inst. Nav. Archit.* 24 (1883) 165–190.
- [2] H. Frahm, Means for Damping the Rolling Motion of Ships., US Patent 970,368 (Sep. 1910).
- [3] H. Frahm, Device for Damping Vibrations of Bodies., US Patent 989,958 (Apr. 1911).
- [4] J. Ormondroyd, J.P. Den Hartog, The theory of the dynamic vibration absorber, *Trans. ASME* 50 (1928) 9–22.
- [5] J. P. Den Hartog, McGraw-Hill, New York, 1957, <https://doi.org/10.1017/s0368393100131049>.
- [6] J. E. Brock, A note on the damped vibration absorber, *J. Appl. Mech.* 284.
- [7] O. Fischer, *J. Wind Eng. Ind. Aerodyn.* 95 (9–11) (2007) 1028–1039, <https://doi.org/10.1016/j.jweia.2007.01.027>.
- [8] P. Dallard, A.J. Fitzpatrick, A. Flint, S. Le Bourva, A. Low, R.M. Ridsdill Smith, M. Willford, The london millennium footbridge, *Struct. Eng.* 79 (22) (2001) 17–21.
- [9] E. S. Taylor, Tech. rep. (Jan. 1936), <https://doi.org/10.4271/360105>.
- [10] M.-N.H. Hamouda, G.A. Pierce, *J. Am. Helicopter Soc.* 29 (3) (1984) 19–29, <https://doi.org/10.4050/jahs.29.19>.
- [11] D. Sauter, P. Hagedorn, *Int. J. Non-Linear Mech.* 37 (8) (2002) 1453–1459, [https://doi.org/10.1016/s0020-7462\(02\)00028-8](https://doi.org/10.1016/s0020-7462(02)00028-8).
- [12] M. Gu, C. Chang, W. Wu, H. Xiang, *J. Wind Eng. Ind. Aerodyn.* 73 (2) (1998) 111–123, [https://doi.org/10.1016/s0167-6105\(97\)00282-1](https://doi.org/10.1016/s0167-6105(97)00282-1).
- [13] A. Casalotti, A. Arena, W. Lacarbonara, *Eng. Struct.* 69 (2014) 62–71, <https://doi.org/10.1016/j.engstruct.2014.03.001>.
- [14] J. Holmes, *Eng. Struct.* 17 (9) (1995) 676–678, [https://doi.org/10.1016/0141-0296\(95\)90027-6](https://doi.org/10.1016/0141-0296(95)90027-6).
- [15] M.G. Soto, H. Adeli, *Archives Comput. Methods Eng.* 20 (4) (2013) 419–431, <https://doi.org/10.1007/s11831-013-9091-7>.
- [16] J. Mayet, H. Ulbrich, *J. Sound Vib.* 333 (3) (2014) 711–729, <https://doi.org/10.1016/j.jsv.2013.09.042>.
- [17] G. W. Housner, Vibration of structures induced by seismic waves, *Shock Vib. Handb.* 3(50).
- [18] Z. Lu, X. Lu, W. Lu, S.F. Masri, *J. Sound Vib.* 331 (9) (2012) 2007–2022, <https://doi.org/10.1016/j.jsv.2011.12.022>.
- [19] A. Thompson, *J. Sound Vib.* 77 (3) (1981) 403–415, [https://doi.org/10.1016/s0022-460x\(81\)80176-9](https://doi.org/10.1016/s0022-460x(81)80176-9).
- [20] G.B. Warburton, *Earthq. Eng. Struct. Dyn.* 10 (3) (1982) 381–401, <https://doi.org/10.1002/eqe.4290100304>.
- [21] A. Kareem, S. Kline, *J. Struct. Eng.* 121 (2) (1995) 348–361, [https://doi.org/10.1061/\(asce\)0733-9445\(1995\)121:2\(348\)](https://doi.org/10.1061/(asce)0733-9445(1995)121:2(348)).
- [22] C. Zang, M. Friswell, J. Mottershead, *Comput. Struct.* 83 (4–5) (2005) 315–326, <https://doi.org/10.1016/j.compstruc.2004.10.007>.
- [23] S. Krenk, J. Høgsberg, *Prob. Eng. Mech.* 23 (4) (2008) 408–415, <https://doi.org/10.1016/j.probenmech.2007.04.004>.
- [24] B. Brown, T. Singh, *J. Sound Vib.* 330 (11) (2011) 2437–2448, <https://doi.org/10.1016/j.jsv.2010.12.002>.
- [25] G. Habib, T. Detroux, R. Vigié, G. Kerschen, *Mech. Syst. Signal Process.* 52–53 (2015) 17–28, <https://doi.org/10.1016/j.ymsp.2014.08.009>.
- [26] S.E. Randall, D.M. Halsted, D.L. Taylor, *J. Mech. Des.* 103 (4) (1981) 908, <https://doi.org/10.1115/1.3255005>.
- [27] E. Pennestri, An application of chebyshev's min–max criterion to the optimal design of a damped dynamic vibration absorber, *J. Sound Vib.* 217 (4) (1998) 757–765.

- [28] G. Calafiore, M.C. Campi, Uncertain convex programs: randomized solutions and confidence levels, *Math. Program* 102 (1) (2004) 25–46, <https://doi.org/10.1007/s10107-003-0499-y>.
- [29] J.Q. Sun, M.R. Jolly, M.A. Norris, *J. Vib. Acoust.* 117 (B) (1995) 234, <https://doi.org/10.1115/1.2838668>.
- [30] T. Asami, O. Nishihara, *J. Vib. Acoust.* 125 (3) (2003) 398, <https://doi.org/10.1115/1.1569514>.
- [31] M.C. Campi, S. Garatti, M. Prandini, The scenario approach for systems and control design, *Ann. Rev. Control* 33 (2) (2009) 149–157, <https://doi.org/10.1016/j.arcontrol.2009.07.001>.
- [32] M.C. Campi, S. Garatti, The exact feasibility of randomized solutions of uncertain convex programs, *SIAM J. Optim.* 19 (3) (2008) 1211–1230, <https://doi.org/10.1137/07069821x>.
- [33] G.C. Calafiore, On the expected probability of constraint violation in sampled convex programs, *J. Optim. Theory Appl.* 143 (2) (2009) 405–412, <https://doi.org/10.1007/s10957-009-9579-3>.
- [34] M.C. Campi, S. Garatti, A sampling-and-discarding approach to chance-constrained optimization: feasibility and optimality, *J. Optim. Theory Appl.* 148 (2) (2010) 257–280, <https://doi.org/10.1007/s10957-010-9754-6>.